

Modeling Interdiffusion Processes in CMSX-10/Ni Diffusion Couple

A. Chyrkin, A. Epishin, R. Pillai, T. Link, G. Nolze, and W.J. Quadackers

(Submitted February 11, 2015; in revised form November 10, 2015; published online January 21, 2016)

A diffusion couple between directionally solidified nickel and the single crystal Ni-base superalloy CMSX-10 was produced by hot pressing in vacuum. The diffusion couples were heat treated at temperatures between 1050 and 1250 °C. The exposed samples were characterized by SEM/EBSD/EPMA. The interdiffusion results in dissolution of the γ' -Ni₃Al in the superalloy and in growth of nickel grains towards CMSX-10. Rapid diffusion of aluminum from the superalloy into pure nickel leads to a significant formation of pores in the superalloy. The interdiffusion processes were modelled using the finite-element simulation software DICTRA with the databases TCNi5 and MobNi2, tailored specially for Ni-base superalloys. The effect of alloying elements on the interdiffusion profiles is discussed in terms of alloy thermodynamics. The calculated element concentration profiles are in good agreement with the EPMA measurements. The interdiffusion modeling correctly predicts the shapes of the concentration profiles, e.g. kinks on the Al and Ti profiles in the vicinity of the original interface in the joint. The calculation predicts with reasonable accuracy the extent and the location of the Kirkendall porosity.

Keywords chemical potential, chemical potential gradients, composition profiles, DICTRA modeling, diffusion, diffusion modeling, electron probe microanalysis (EPMA)

1. Introduction

Ni-base superalloys^[1] are widely used as construction materials in land-based gas turbines and aero-engines, in particular, in the production of poly- as well as single-crystalline blades. The blades operate under extremely intensive mechanical and thermal load, which requires high mechanical strength and corrosion resistance of these materials. The remarkable creep resistance of the Ni-base superalloys largely relies on precipitate strengthening by the intermetallic γ' -Ni₃(Al/Ti/Ta) phase. The γ/γ' -microstructure strongly depends on the actual alloy composition and heat treatment. The newer generation of single-crystal Ni-base superalloys such as CMSX-4 or CMSX-10 typically have in their microstructure 0.5 μm thick cuboids of the γ' -precipitates imbedded in the γ -matrix.^[2] The γ -layers between the intermetallic particles are usually 50 nm thick.

Information from this article was originally presented at DIMAT 2014, held in Münster, Germany, August 17–22, 2014, and has been expanded from the original presentation.

A. Chyrkin, R. Pillai, and W.J. Quadackers, Institute for Energy and Climate Research (IEK-2), Forschungszentrum Jülich GmbH, Leo-Brandt-Straße, 52425 Jülich, Germany; A. Epishin and T. Link, Technical University of Berlin, Ernst-Reuter-Platz 1, 10587 Berlin, Germany; G. Nolze, Federal Institute for Materials Research and Testing (BAM), Unter den Eichen 87, 12205 Berlin, Germany. Contact e-mail: a.chyrkin@fz-juelich.de.

Apart from the precipitate strengthening, Ni-base superalloys are also solid-solution strengthened by alloying with the refractory metals such as Re, W, Mo, etc. The refractories are known to improve creep strength and increase the melting point of the superalloy.^[1]

The thermo-mechanical stability of the γ/γ' -microstructure over time may be affected by oxidation^[3] or interdiffusion^[4] related compositional changes in the alloy during service. The oxidation/interdiffusion-induced loss of creep strength of the Ni-base superalloys is mainly associated with the dissolution of the γ' -phase and, hence, the loss of the γ/γ' -microstructure. The new generation single-crystal Ni-base superalloys contain relatively low amounts of Al and/or Cr with the result that they may provide a poor oxidation/corrosion resistance.^[3,5,6] Therefore Al/Cr-rich oxidation/corrosion resistant overlay coatings are usually applied to the blade surfaces. Additionally, welding of different Ni-base superalloys is common in the gas turbine technology. The interaction between chemically different alloys leads to interdiffusion, which may have detrimental consequences for the superalloy microstructure, mechanical properties and, eventually, material performance.

The interdiffusion processes between two different Ni-base alloys or between a Ni-base superalloy and a corrosion resistant coating system may lead to the degradation of the superalloy microstructure and consequently to the loss of creep resistance. Among possible interdiffusion related degradation mechanisms the following phenomena have been observed and documented: (i) γ' -dissolution/coarsening,^[4] (ii) void formation (Kirkendall effect),^[7] (iii) formation of brittle TCP (topologically closed packed) phases rich in refractory metals at the weld/coating interface.^[8,9]

In general practice, the evaluation of the chemical compatibility of Ni-base superalloys with different types of coatings involves tedious and time consuming

experimental testing. Predictive thermo-kinetic modeling based on the CALPHAD approach can be a reasonable alternative to extensive testing programs. However, the accuracy of these calculations depends on the available thermodynamic and kinetic data, which are subject to permanent optimization.^[4,10-13]

In the present paper the interdiffusion processes in a diffusion couple in which nickel is welded with the single-crystal Ni-base superalloy CMSX-10 are modeled using the homogenization approach^[14] developed by Thermo-Calc. The aim of the study was to quantitatively predict the compositional and microstructural changes occurring in the superalloy during interdiffusion.

2. Experimental Procedure

The diffusion couple studied was manufactured from the 3rd generation Ni-base single-crystal superalloy CMSX-10^[2] and directionally solidified (DS) high-purity nickel. The nominal chemical composition of CMSX-10 is listed in Table 1. The CMSX-10 ingot was cast in an industrial set-up for single-crystal blade production and subsequently subjected to a standard ten-step solution anneal heat-treatment for 45 h in the temperature range 1315-1365 °C^[15] and following a subsequent ageing treatment: 1150 °C/4 h, 870 °C/24 h, 760 °C/30 h. After the heat treatment, the superalloy has a specific cuboidal γ/γ' -microstructure. The γ' cuboids are approximately 500 nm thick and are separated from each other by a 50 nm thick layer of the γ phase. Schulze and Feller-Kniepmeier^[16] estimated the γ' volume-fraction in CMSX-10 after standard heat treatment to be approximately 80%. The other part of the diffusion couple was high-purity nickel obtained by zone melting. The Ni samples contained a few mm thick columnar grains.

The diffusion couples were manufactured from 2.5 mm thick discs cut from the alloy bars. The discs were ground with abrasive papers on both sides and subsequently polished on one side with diamond pastes to 1 μ m surface finish. The polished discs were diffusion welded in a high-temperature universal testing machine MTS 810 with inductive sample heating at 1050 °C, under compressive pressure of 10 MPa, for 1 h. The atmosphere pressure in the evacuated chamber was 10⁻⁶ mbar. After diffusion welding

the samples were cut to control the quality of the weld interface using secondary electron microscopy (SEM).

The diffusion couples were subjected to high-temperature annealing in evacuated ampules at 1050, 1150, and 1250 °C. The ampules were air cooled, the cooling rate being approximately 2 K per second. The annealing times were 3072, 768, and 192 h, respectively. The interdiffusion times were selected for two reasons. First, the penetration depth of the slowest diffusing species, i.e., Re, has to be at least 100 μ m to assure reliable electron probe microanalysis (EPMA) profile measurement. Second, the annealing tests were designed so that the total mass transfer in all three samples was approximately of the same order of magnitude. After annealing the diffusion couples were cut perpendicular to the interface and cross-sectioned using the standard metallographic preparation technique. The microstructure of the interdiffusion zone was characterized using optical microscopy (Zeiss AxioScope) and scanning electron microscopy (LEO GEMINI 1530 VP). The crystallographic orientation of the observed phases in the interdiffusion zone was determined with the electron backscatter diffraction (EBSD) detector e-Flash HR using ESPRIT and CrystAlign software. The element concentration profiles were measured by the wavelength x-ray dispersive (WDX) microanalyzer JXA8900, Jeol, by performing 1.5 mm long EPMA line scans perpendicular to the weld interface with 5 μ m step size.

3. Modeling Procedure

The coupled thermodynamic-kinetic approach known as the homogenization model^[14] served as the basis to model the interdiffusion processes in the CMSX-10/Ni diffusion couple. This approach allows the transformation of a multicomponent, multiphase problem into a single-phase 1D problem. The sample geometry is discretised into a suitable number of volume cells. The phase fractions, compositions and chemical potentials are defined by the local equilibrium resulting due to element concentrations, temperature and pressure in one volume cell.

The homogenisation model is based on the phenomenological treatment of diffusion by Onsager.^[17] The flux of a species k in mole m⁻² s⁻¹ is given as

Table 1 Chemical composition of single-crystal Ni-base superalloys CMSX-10 and polycrystalline superalloy René-88

Element	Al	Ti	Cr	Co	Ni	Nb	Mo	Hf	Ta	W	Re
CMSX-10 ^[2]											
Nominal chemical composition											
wt.%	5.7	0.2	2	3	Bal.	0.1	0.4	0.03	8	5	6
at.%	13.2	0.3	2.4	3.2	Bal.	0.06	0.3	0.01	2.8	1.7	2.0
EPMA (input for modelling)											
at.%	14.0	0.3	2.8	3.6	Bal.	...	0.25	...	2.8	1.7	2.0
René-88 ^[36]											
at.%	4.5	4.5	18	13	Bal.	0.5	2.5	1.3	...

$$J_k = -c_k M_k \frac{\partial \mu_k}{\partial z}. \quad (\text{Eq 1})$$

Here c_k is the molar concentration of k in mol m^{-3} , μ_k the chemical potential in J mol^{-1} , z the space coordinate in m . The atomic mobility M_k is directly related to the tracer diffusivity D_k^* by means of the Einstein relation

$$D_k^* = RTM_k, \quad (\text{Eq 2})$$

where T is absolute temperature and R the universal gas constant.

In the homogenization model^[14,18] the flux is derived from the absolute reaction rate theory as

$$J_k = -\frac{RT}{\bar{V}_m \Delta \bar{z}} \sqrt{[M_k x_k]_{n-1}^{eff} [M_k x_k]_n^{eff}} 2 \sinh\left(\frac{\Delta \mu_k}{2RT}\right). \quad (\text{Eq 3})$$

Here \bar{V}_m is the partial molar volume of the species k , $\Delta \bar{z}$ the width of the volume cell, $n \in [0, K]$ is the volume element number, K being the number of computational nodes, $\Delta \mu_k$ the difference in chemical potential of the species k between the adjacent nodes n and $n-1$; \sinh is the hyperbolic sine function. The product $[M_k x_k]^{eff}$ is the effective mobility of the species k in the multiphase alloy. Various alternatives to evaluate the local effective kinetic properties such as mobilities are documented in Ref 14. In the present paper, the ‘‘Rule of Mixtures’’ has been used, considering diffusion in the γ -FCC (disordered solid solution) and γ' -FCC_L12 (ordered compound with a narrow range of homogeneity) phases. The main advantage of this approach is the straightforward solution of the diffusion problem in multiphase systems such as γ/γ' Ni-base superalloys because diffusion in all stable phases is taken into account. This is contrary to the spheroidal dispersion approach in which diffusion is considered to occur only in the matrix phase (e.g. γ -FCC) while the precipitate phases such as carbides, γ' -Ni₃Al or β -NiAl serve as point sinks in local equilibrium with the matrix phase.^[4,19,20] In the dispersion model a so-called labyrinth factor is usually introduced to account for the blocking effect of the non-diffusion precipitate phases on the mass transport. The labyrinth factor is a function of the volume-fraction of the precipitate phases. The dispersion approach is generally acknowledged to accurately describe processes in which diffusion occurs mainly in the metallic matrix phase such as carburization^[20,21] and/or nitridation.^[22] However, in such multi-phase alloy system as (Ni,Co)CrAlY coatings (γ/β) and/or Ni-base superalloys (γ/γ') the fraction of the intermetallic phase may amount to 70-80 vol.% and, hence, the mass transport in these phases cannot be ignored.

The interdiffusion calculations were performed using the software DICTRA,^[23] in which the homogenisation model is implemented. Thermodynamic and kinetic data were taken from the TCNi5^[24] and MobNi2^[25] databases, respectively. The boundary condition for both ends of the diffusion couple was set as a zero-flux plane. The width of the diffusion couple was assumed to be 4 mm. The measured average chemical composition of CMSX-10 in

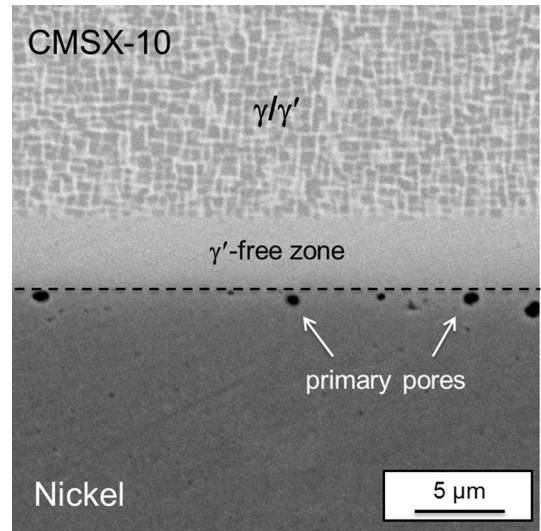
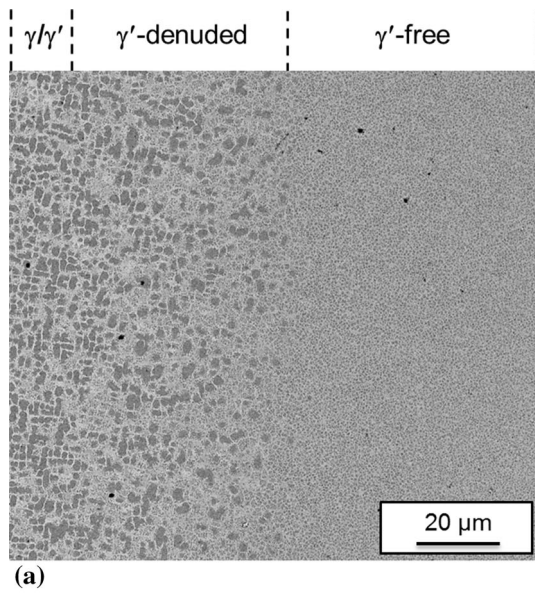


Fig. 1 Microstructure of CMSX-10/Ni diffusion couple after hot pressing under 10 MPa at 1050 °C for 1 h in vacuum. Dashed line indicates weld interface

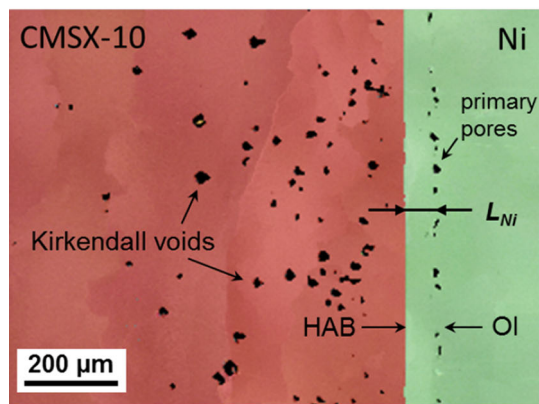
the as-received state (Table 1) was used as the initial composition of the superalloy at $t = 0$.

4. Results

The microstructure of the CMSX-10/Ni weld is shown as a backscattered SE image in Fig. 1. The superalloy part of the diffusion couple reveals a typical cuboidal γ/γ' microstructure. The nickel grain is the darker phase at the bottom of the BSE image. A bright strip between CMSX-10 and the nickel grain is the γ' -free region in the superalloy. It formed during welding due to Al diffusion into the nickel grain. The width of this layer ($L_{\gamma'}$) is approximately 4 μm after 1 h diffusion welding at 1050 °C. A number of small voids, approximately 1 μm in diameter, were observed at the interface between the γ' -free zone and the nickel grain. These voids form during the welding process at the original weld interface and serve as a marker in the further microstructural analyses. The void formation is probably the result of incomplete bonding. Much bigger voids, 15-20 μm in diameter, were detected in the superalloy after annealing (Fig. 2). Since the microstructural changes in all three diffusion couples CMSX-10/Ni are qualitatively identical, only the 1250 °C/192 h anneal is further discussed in detail because the effects observed were most pronounced in this test. Three major microstructural effects can be identified: (i) formation of a zone in the superalloy in which dissolution of the γ' -phase occurs (Fig. 2a); (ii) growth of the Ni grain towards CMSX-10 (Fig. 2b); (iii) significant Kirkendall porosity^[7,26] in CMSX-10 (Fig. 3a). All three microstructural observations are related to the rapid diffusion of Al from the superalloy into the nickel. The widths of the γ' -free zone $L_{\gamma'}$ after the various exposures were determined from the SEM images and are listed in Table 2.



(a)

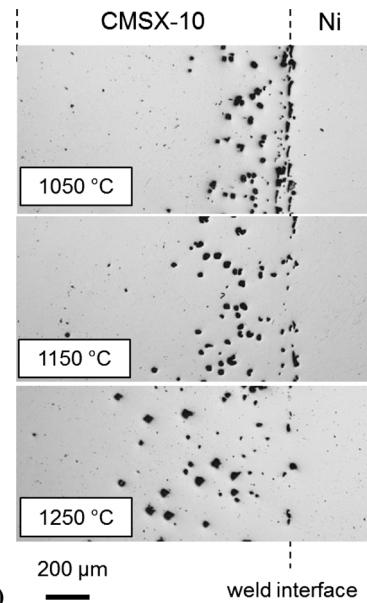


(b)

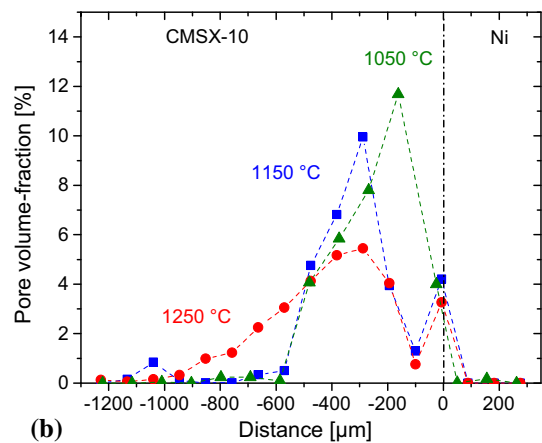
Fig. 2 Microstructure of the interdiffusion zone in CMSX-10/Ni diffusion couple after 192 h annealing at 1250 °C: (a) BSE image of the macroscopic interface γ/γ' - γ ; (b) EBSD mapping showing the interface (HAB) migration from Ni (green) towards CMSX-10 (red) during interdiffusion (Color figure online)

The growth of the nickel grain is presumably driven by the reduction in grain boundary free energy as the HAB grows into the superalloy. As can be seen in Fig. 2(b), the grain growth has removed the Kirkendall porosity between the primary porosity and HAB since the grain growth recrystallizes the nickel and thus may repair imperfections. The EBSD mappings in Fig. 2(b) revealed that the CMSX-10 single-crystal orientation perpendicular to the interface plane is close to [001]. The nickel grain orientation deviates by 10°-20° from this direction. The interface displacements L_{Ni} , the distance between the high-angle boundary and the primary porosity (see Fig. 2b), were measured from the EBSD mappings and are also listed in Table 2.

The Kirkendall void formation is illustrated in Fig. 3(a) with the optical micrographs of the annealed diffusion couples. The void volume-fraction profiles obtained using



(a)



(b)

Fig. 3 Kirkendall void formation in CMSX-10/Ni diffusion couple after annealing at different temperatures: (a) light microscope images of pores in superalloy, (b) pore volume-fraction profiles across the diffusion couple

an image analysis technique revealed two relative maxima (see Fig. 3b). The smaller peak on the right side of each profile is related to the primary porosity at the weld interface. The primary pores grew during the diffusion welding while the secondary pores appeared in the superalloy after the long-term exposures. The left peak relates to the secondary porosity. The maximum of the void volume-fraction is the highest for the lowest annealing temperature, 1050 °C, while its width is the largest for the 1250 °C anneal.

The element concentration profiles across the diffusion couple are plotted in Fig. 4. In the γ/γ' two-phase region the data scatter is expectedly high because of the different compositions of the γ and γ' phases. In the single-phase region, the shapes of the interdiffusion profiles are different for the elements which solubility is higher in the γ -phase

Table 2 Annealing parameters of CMSX-10/Ni diffusion couple and measured zone widths and rates for γ' -free zone (L_γ) thickening and nickel grain growth (L_{Ni})

T, °C	T, h	L_γ , μm	L_{Ni} , μm	ζ_γ , $\text{m}^2 \text{s}^{-1}$	ζ_{Ni} , $\text{m}^2 \text{s}^{-1}$
1050	3072	500	50	4.2×10^{-15}	2.3×10^{-16}
1150	768	300	63	3.2×10^{-14}	1.4×10^{-15}
1250	192	215	72	3.6×10^{-13}	7.5×10^{-15}

such as Co, Cr, W, Mo, Re, and the elements which tend to dissolve in the γ' -phase such as Al, Ti and Ta. The elements preferentially dissolved in the γ -phase show a classical error-function type interdiffusion profile. In contrast to the main elements dissolved in the γ -phase, the profiles of the γ' -stabilizing elements, Al, Ta, and Ti, exhibit a kink or even a nearly flat plateau in the vicinity of the original weld interface (Fig. 4). The shape of the interdiffusion profiles will be discussed in detail.

5. Discussion

5.1 Dissolution of γ' -Phase

The extensive γ' -dissolution in the superalloy part of the diffusion couple (Fig. 2a) occurs as a result of rapid Al diffusion into the pure nickel. The γ' -dissolution has been reported to occur as the consequence of aluminium depletion due to interdiffusion^[27] or oxidation.^[3] Similar to the aforementioned studies, in the present work the γ' to γ transformation was taken into account in the interdiffusion modelling under assumption of local equilibrium across the diffusion couple. Additionally, diffusion in the γ' -phase is explicitly calculated in the homogenization model, which made the use of the labyrinth factor^[19] in the calculation obsolete.

It should be mentioned that a minor fraction of the small (0.1 to 0.4 μm in size) γ' -particles re-precipitated in the γ' -free zone of the superalloy on cooling to room temperature (Fig. 2a). The size and morphology of these new γ' -particles distinctly differ from the original cuboid precipitates in the γ'/γ' microstructure and suggest that the microstructure formed during cooling. The diffusion distance of Al in the 1250 °C diffusion couple is approximately 500 μm while the distance between precipitates is of the order of several μm . Assuming a diffusion time on cooling to be one minute and then comparing a ratio of square root of times (heat treatment/cooling) to the ratio of diffusion distances (γ' -dissolution zone/distance between particles), one obtains a similar ratio of 100 to 200. This calculation confirms the assumption that the secondary γ'/γ' -microstructure in Fig. 2(a) is the result of γ' precipitation on cooling in the areas of Al supersaturation close to the γ' -dissolution front.

The calculated γ' -depletion profiles are plotted in Fig. 5(a). As can be seen in the SEM images (Fig. 2a), the γ' -dissolution is gradual, i.e., there is no sharp jump between the two-phase γ'/γ' and the single-phase γ -region. The predicted widths of the γ' -free zone are in excellent agreement with the experimental values. The growth rate

constants ξ_i of the γ' -free zone growth were calculated using the parabolic rate expression

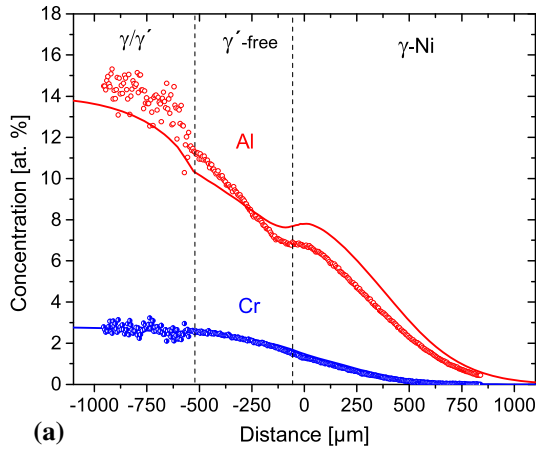
$$\xi_i = \frac{L_i^2}{t} \quad (\text{Eq 5})$$

and are listed in Table 2. In Eq 5 index i relates either to the γ' -free zone (γ) or to the interface displacement (Ni). The growth rates of the nickel grain width ξ_{Ni} were estimated in the same manner. The temperature dependence of ξ_γ and ξ_{Ni} is plotted in Fig. 5(b). The activation energy of the interface displacement is 293 kJ/mole, which is close to the value for nickel self-diffusion (287 kJ/mole).^[28] The activation energy for the γ' -dissolution in the superalloy is 372 kJ/mole.

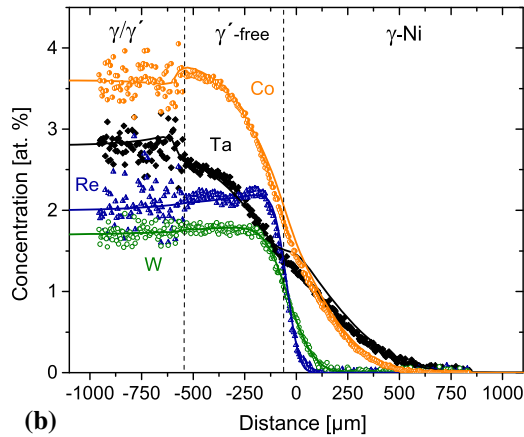
5.2 Interdiffusion Profiles

The most interesting finding in the present work was the shape of the interdiffusion profiles of the γ' -stabilizing alloying elements Ti, Ta, Al. They display a kink or even a nearly flat plateau near the original diffusion couple interface (Fig. 4). Especially pronounced is this effect for aluminium (Fig. 4a). A locally lower concentration gradient in an interdiffusion profile implies a faster diffusion of the respective species at this location. In order to understand the nature of this enhanced diffusion of the γ' -stabilizers, homogenization calculations were performed. The calculated concentration profiles are plotted in Fig. 4 as solid lines. The interdiffusion modelling quantitatively predicted all experimentally observed trends. The interdiffusion of the γ -matrix stabilizing elements such as cobalt, chromium, tungsten, and molybdenum is well described by the error-function type profiles with reasonable accuracy. The Re interdiffusion profile differs from the rest of the γ -matrix stabilizing elements; it shows a slight enrichment in the γ' -free zone in the diffusion couple. The rhenium enrichment is explained by its extremely low diffusivity in nickel.^[29-31] As the other alloying elements migrate into the nickel grain, the concentration of the substantially less mobile Re locally increases with respect to nickel. The calculated Re profile in Fig. 4(b) correctly predicted the Re enrichment near the diffusion couple interface. The calculated concentration profiles of all three γ' -stabilizing elements, Al, Ta, and Ti, have a similar shape. The Al and Ti profiles show local concentration minima and maxima close to the diffusion couple interface. The calculated Ta profile shows only a weak kink.

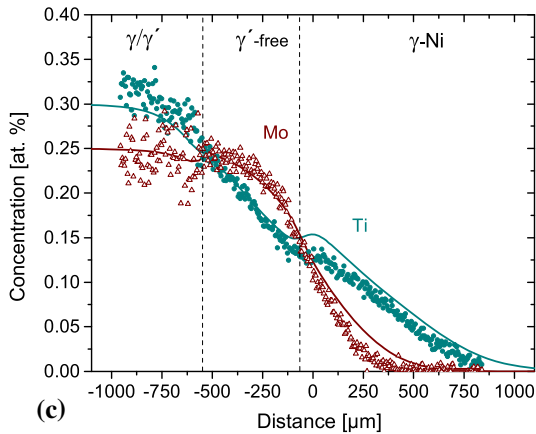
Thompson and Morral^[32-35] showed that in ternary alloys the shape of the penetration profiles is determined by the composition vector orientation assuming constant diffusivity. The authors classified the interdiffusion profiles as the



(a)



(b)

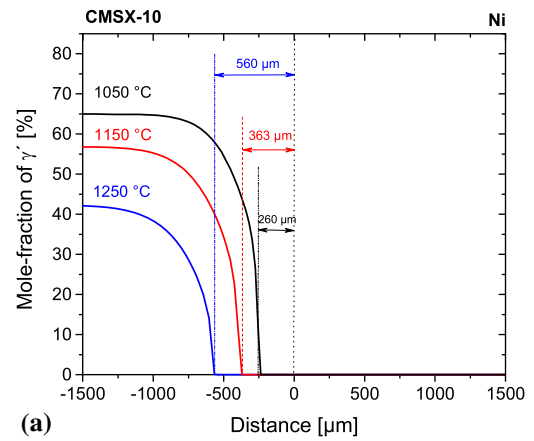


(c)

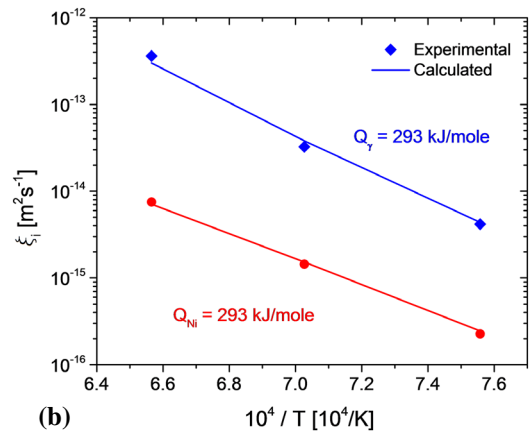
Fig. 4 Concentration profiles in diffusion couple CMSX-10/Ni after annealing for 192 h at 1250 °C. The dots are experimental data obtained by EPMA; the lines are calculated interdiffusion profiles: (a)—Al, Cr; (b)—Co, Ta, W; (c)—Mo, Ti

penetration curves having extrema and those without extrema. The shapes of the interdiffusion profiles obtained numerically in the present work can be regarded as Type II penetration curves from Ref 32.

Very similar concentration profiles of Al and Ti were reported by Campbell et al.^[36] in a Ni/René-88 diffusion



(a)



(b)

Fig. 5 Calculated γ' -dissolution profiles (a). Vertical lines indicate position of the γ - γ' interface determined experimentally. (b) Temperature dependence of the thickening rate of the γ -zone (blue line and dots) and the growth rate of the Ni-crystal (red line and dots) (Color figure online)

couple annealed for 1000 h at 1150 °C. Moreover, the experimentally measured Al and Ti concentration profiles in the present study also exhibited a kink (Ti) or plateau (Al). The shape of the calculated and measured Al/Ti profiles in the Ni/René-88 diffusion couple^[36] supports the hypothesis of enhanced diffusion of the γ' -stabilizing elements at the diffusion couple interface. In order to understand the nature of the enhanced diffusion, Eq 1 has to be re-written in terms of interdiffusion coefficients and concentrations

$$J_k = -\tilde{D}_{kk}^j \frac{\partial C_k}{\partial z} - \tilde{D}_{kj}^j \frac{\partial C_j}{\partial z} - \dots \quad (\text{Eq 6})$$

Equation 6 implies that each element in a multicomponent diffusion couple, e.g., CMSX-10/Ni, is diffusing not only under the driving force resulting from its own concentration gradient, but also from the concentration gradients of the other alloying elements. In other words, referring to Eq 1 and 3, the chemical potential of element k is a function of the concentrations of all alloying elements $\mu_k = f(p, T, c_1, c_2 \dots)$. The enhanced diffusion in the

concurrent chemical gradients has been observed, for example, in Ref 37,38 in the alloy systems Ni-Cr-Si/Al and Ni-Al-Re/W. From the prospective of diffusion in the concurrent chemical gradients, the observed interdiffusion profile with a kink can be regarded as a sum of $n-1$ error-functions (n = number of species) as described in references.^[32,39] The main contribution to the interdiffusion profile of this type is provided by the main interdiffusion coefficient term \bar{D}_{kk}^i , i.e. one of the eight Eigen-values of the diffusivity matrix $[D]$. The error-functions with the largest Eigen-value tends to dominate the interdiffusion profile and is strongly influenced by the elements with the largest diffusivity, Al in the present case. The error-function with

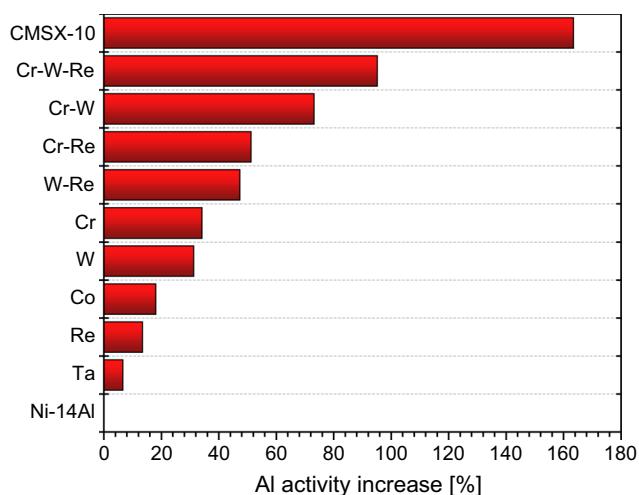


Fig. 6 Effect of alloying elements on chemical activity of Al in nickel. The increase of the Al activity was calculated using Thermo-Calc for a number of model compositions at 1250 °C and related to the Al activity in an imaginary binary Ni-14(at.%)Al alloy at the respective temperature (see also Table 3). The total effect of the alloying elements in a superalloy is represented by the highest column for CMSX-10

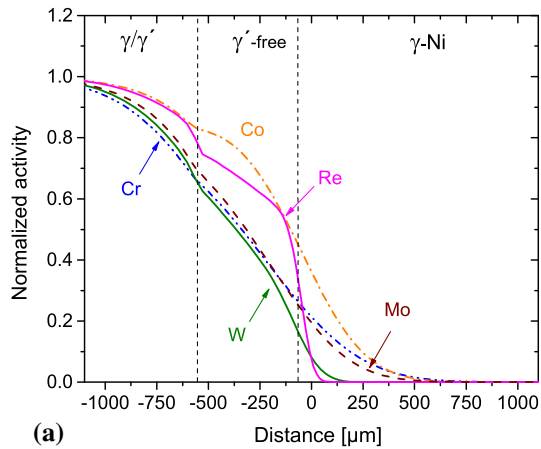
the smaller Eigen-values are important near the diffusion couple interface ($x = 0$) and can cause kinks.^[32,39] These error-functions are associated with the slower moving species such as W and Re.

It is important to understand which alloying element in CMSX-10 established an additional chemical potential gradient across the diffusion couple and is responsible for the kink/plateau formation (Fig. 4). The effect of the alloying elements on the chemical activity of Al was estimated by calculating the thermodynamic equilibria in Thermo-Calc. For the sake of clarity, the hypothetical ternary, quaternary, etc. alloys simulating the CMSX-10 composition are compared with an imaginary binary Ni-14Al (at.%) alloy. The increase of the Al activity due to alloying elements is summarized in Fig. 6 and Table 3. First, all studied alloying additions, especially chromium and tungsten, tend to increase the Al activity in nickel. Second, the alloying effects seem to be additive. Third, the Al activity in CMSX-10 is by a factor of 2.6 higher compared to that in the binary Ni-14Al alloy. It implies that aluminium would migrate from the superalloy into Ni-14Al although there would be no concentration gradient in such a diffusion couple.

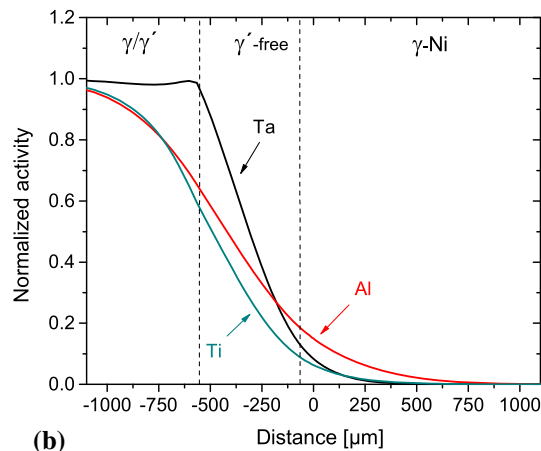
Now the interdiffusion profiles of the slow diffusing refractory metals, tungsten and rhenium, have to be considered (Fig. 4). The diffusion distances of these two species are small compared to that of Al and to the width of the γ' -free zone. Compared to Al, the elements tungsten and rhenium are virtually immobile. The Al concentration at the beginning of the plateau area is approximately 7 at.% while the W and Re concentrations remain almost unchanged (Fig. 4). Re is even slightly enriched due to the Al depletion at this site. This implies that the Al activity in the superalloy close to the weld interface is higher than it would be in the corresponding binary Ni-14Al alloy, i.e., the alloy without slow diffusion species that increase the Al activity in Ni. The slow diffusion of Re and W thus creates an additional chemical potential gradient for Al, resulting in enhanced Al diffusion at the weld interface and the characteristic interdiffusion profile shape. The calculated chemical poten-

Table 3 Calculated effect of alloying elements on Al activity in imaginary Ni-Al-X alloys (concentration in at.%) at 1250 °C. Activities with reference to liquid phase were computed using Thermo-Calc with TTNI7 database^[40]

	Concentrations, at.%							Al activity $\times 10^5$
	Al	Cr	Co	Ni	Ta	W	Re	
No addition	14	Bal.	3.38
Cr	14	2.8	...	Bal.	4.54
Co	14	...	3.6	Bal.	4.00
Ta	14	Bal.	2.8	3.61
W	14	Bal.	...	1.7	...	4.44
Re	14	Bal.	2.0	3.84
W-Re	14	...	W-Re	Bal.	...	1.7	2.0	4.98
Cr-Re	14	2.8	...	Bal.	2.0	5.12
Cr-W	14	2.8	...	Bal.	...	1.7	...	5.86
Cr-W-Re	14	2.8	...	Bal.	...	1.7	2.0	6.60
CMSX-10	14	2.8	3.6	Bal.	2.8	1.7	2.0	8.91



(a)

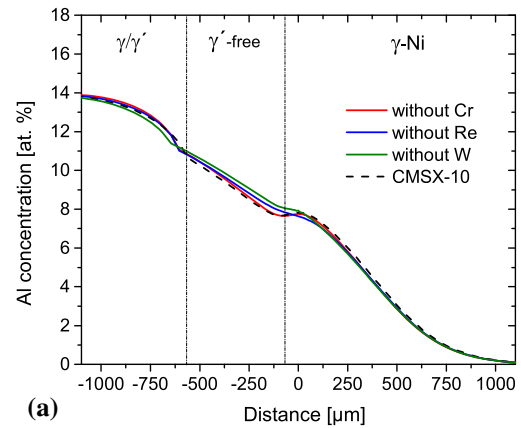


(b)

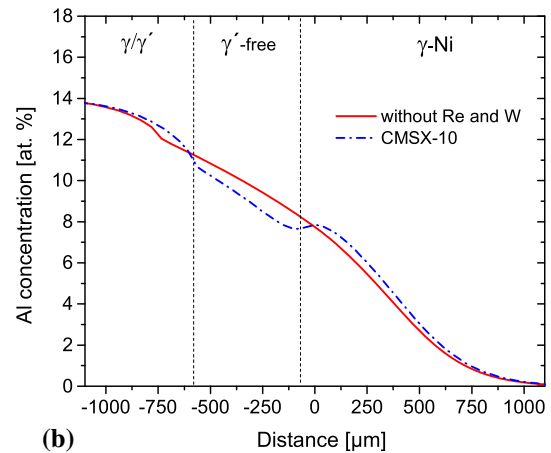
Fig. 7 Calculated normalized chemical activity profiles in diffusion couple CMSX-10/Ni after 1250 °C/192 h annealing. (a) γ -matrix stabilizing elements, (b) the γ' -stabilizers

tial profiles of the alloying elements in CMSX-10 are plotted in Fig. 7. For easier comparison of the values, the data were normalized to unity with respect to their activities in the superalloy prior to annealing. It is worth noting that the Al activity profile is an error-function type curve while the matrix element profiles show a kink at the γ/γ' -interface. The activity profiles of W and Re are substantially steeper than the corresponding concentration profiles. This is related to the reciprocal effect of Al depletion on the activity of these elements. The same considerations should apply to the other γ' -elements Ta and Ti.

To verify this hypothesis, a number of interdiffusion simulations were carried out, in which the composition of CMSX-10 was reduced by one or two alloying elements. The resulting Al profiles are plotted in Fig. 8. As follows from the calculated profiles in Fig. 8(a), removal of only one alloying element from CMSX-10 has virtually no effect on the shape of the Al profile. The kink is less pronounced if W or Re is taken out from the alloy, however, it does not vanish completely. If both slow diffusing species are removed from the alloy, the kink disappears: the Al profile is then an error-function type curve (Fig. 8b).



(a)

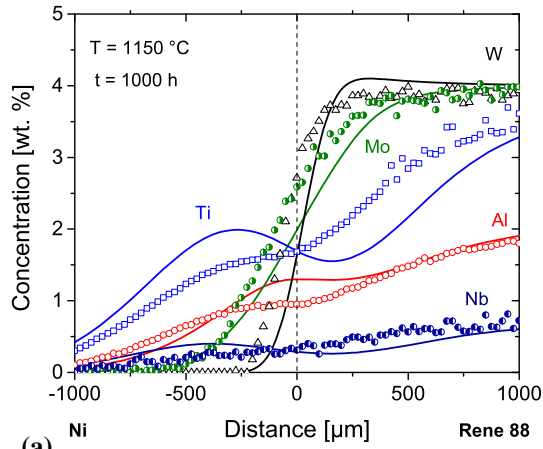


(b)

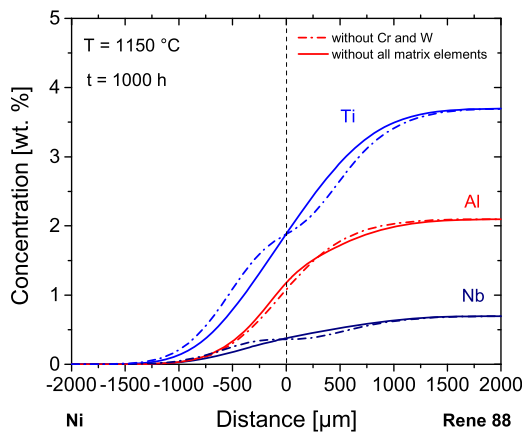
Fig. 8 Calculated Al concentration profiles in diffusion couple CMSX-10/Ni after 1250 °C/192 h annealing. In (a), single alloying elements were eliminated from the CMSX-10 composition, in (b) Re and W simultaneously, until the Al profile converged into an error-function type curve

A similar analysis was applied to the data from Ref 36. The interdiffusion profiles in the Ni/René-88 diffusion couple were re-calculated in the present work using the more recent databases TTNI7^[40] and MobNi1.^[41] The newly calculated profiles qualitatively confirmed the findings of Ref 36. Together with the experimental measurements they are plotted in Fig. 9(a). René-88 contains substantially more Cr than CMSX-10. Chromium is known to affect Al activity^[42,43] and thus its diffusion^[37] in Ni-base alloys. Therefore Cr was also added to the list of elements, which are subject to composition reduction analysis. Similar to the case of CMSX-10, the composition reduction of the imaginary superalloy results in the error-function type concentration profiles of the γ' -elements such as Al, Ti and even Nb (Fig. 8b). However, in this case all γ -matrix stabilizing elements have to be removed from René-88 to obtain this effect.

The composition reduction analysis applied to the interdiffusion calculation revealed a correlation between the shape of the γ' -stabilizing element interdiffusion profiles and the chemical interaction of these species with



(a)



(b)

Fig. 9 Calculated and measured (EPMA data from Ref 36) concentration profiles in diffusion couple Ni/René-88 (a). Concentration profiles of the γ' -stabilizing elements after composition reduction analyses (b)

the γ -matrix stabilizing elements in Ni-base superalloys. Although the calculations explain the interdiffusion mechanisms in such a complex system like a CMSX-10/Ni joint, more experimental data are necessary to prove the interpretation of the unconventional shape of the interdiffusion profiles discussed in this work and improve the agreement between modelling and experiment.

5.3 Secondary Porosity

The reason for the abundant void formation in the superalloy (Fig. 3) is that Al more rapidly diffuses from CMSX-10 into the nickel than the other elements. To describe this phenomenon quantitatively, the fluxes of the diffusing species have to be compared. The calculated fluxes for all alloy constituents are plotted in Fig. 10. The calculation results show that the aluminium flux J_{Al} into pure nickel is not compensated by the nickel flux J_{Ni} into CMSX-10. Compared to those of Al and Ni, the fluxes of the other alloy species are negligibly small. For an alloy

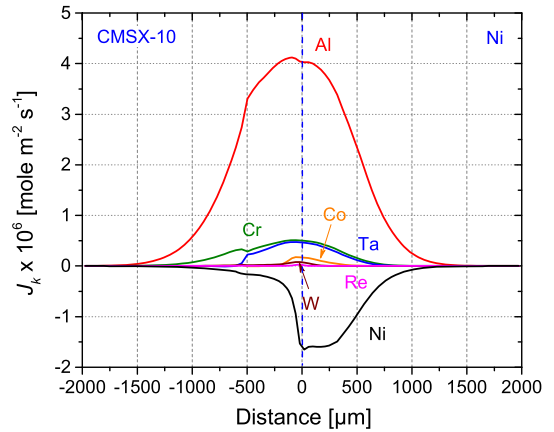


Fig. 10 Calculated intrinsic fluxes (J_k) of the diffusing species in diffusion couple CMSX-10/Ni after 192 h annealing at 1250 °C

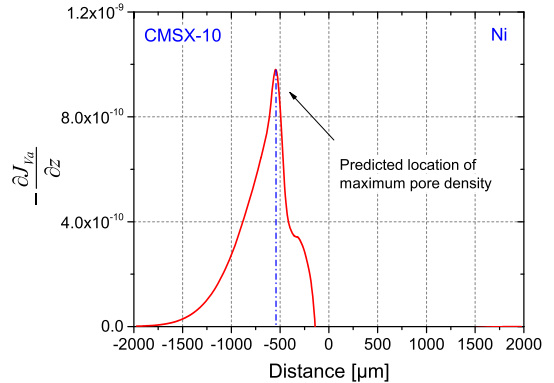


Fig. 11 Gradient of vacancy flux ($-\frac{\partial J_{va}}{\partial z}$) in CMSX-10/Ni diffusion couple as function of distance after 192 h annealing at 1250 °C. The calculation predicts maximum pore density to be located at the γ/γ' - γ interface in CMSX-10

system containing N elements, the flux of vacancies can be defined as

$$J_{Va} = - \sum_{k=1}^N J_k. \quad (\text{Eq 7})$$

According to Höglund and Ågren,^[7] high positive values of the quantity ($-\frac{\partial J_{va}}{\partial z}$) are indicative of pore formation. The vacancies are enriched in the γ' -free region while the available sinks are not strong enough to sustain sufficiently high annihilation rates, and thus the resulting local vacancy supersaturation leads to formation of pores (Fig. 3). The function ($-\frac{\partial J_{va}}{\partial z}$) was calculated on the basis of the intrinsic fluxes from Fig. 10 and plotted in Fig. 11. The predicted maximum pore density is located close to the γ' -dissolution front after 192 h exposure at 1250 °C (560 μm from the original interface). The vacancies seem to condense at the

γ/γ' - γ interface while the interface itself is moving into the superalloy interior.

The primary pores at the original weld interface (Fig. 1) were also found to grow during isothermal annealing, obviously, because of the enhanced Al diffusion in this region not matched by the corresponding outward Ni flux. The vacancies generated close to the weld interface condense on the surface of the primary pores and increase thus their size.

6. Summary and Conclusions

The interdiffusion processes in a CMSX-10/Ni diffusion couple were studied in the temperature range 1050-1250 °C. Rapid diffusion of Al from the superalloy into the nickel results in the formation of a wide γ' -free zone in the superalloy and abundant porosity due to vacancy condensation. Two types of porosity were found: the primary pores at the weld interface and the secondary pores in the Ni-base superalloy. The element interdiffusion profiles between CMSX-10 and nickel can be divided into two groups. The elements with a high solubility in the γ -phase form classical error-function type concentration profiles in the single-phase region. In contrast, the interdiffusion profiles of the γ' -stabilizing species such as Al, Ta and Ti, reveal a kink or even a flat plateau in the vicinity of the weld interface. The thermo-kinetic interdiffusion modelling correctly predicted the γ' -dissolution rates and the locations of the most pronounced porosity. More importantly, the modelling correctly predicted the shapes of the experimental interdiffusion profiles. The kinks on the Al, Ti, and Ta profiles were shown to stem from the interaction between γ' - and γ -stabilizing elements in the nickel matrix. The γ' -stabilizing elements diffuse in their own concentration gradient and in several gradients of slow diffusing elements such as Re or W. The resulting concentration profile is thus the sum of eight error-functions, which gives rise to a kink/plateau in the zone close to the original weld interface ($x = 0$). The interdiffusion calculations with the imaginarily reduced CMSX-10 composition eliminating Re and W resulted in kink free, error-function type concentration profiles of the γ' -stabilizing elements. The similar composition reduction analysis applied to the diffusion couple Ni/René-88^[36] revealed the same tendency. The elimination of all γ -stabilizing matrix elements from the simplified superalloy composition leads to an error-function type of the concentration profiles of the γ' -stabilizing elements Al, Ti, and Nb.

References

1. R.C. Reed, *The Superalloys: Fundamentals and Applications*, Cambridge University Press, Cambridge, 2006
2. G.L. Erickson, The development and application of CMSX (R)-10 (1996)
3. M. Bensch, J. Preussner, R. Huttner, G. Obigodi, S. Virtanen, J. Gabel, and U. Glatzel, Modelling and Analysis of the Oxidation Influence on Creep Behaviour of Thin-Walled Structures of the Single-Crystal Nickel-Base Superalloy Rene N5 at 980 °C, *Acta Mater.*, 2010, **58**, p 1607-1617
4. K.V. Dahl, J. Hald, and A. Horsewell, Interdiffusion between ni-based superalloy and MCrAlY coating, *Diffusion in Solids and Liquids—Mass Diffusion*, A. Öchsner and J. Grácio, Ed., Trans Tech Publications Ltd, Stafa-Zurich, 2006, p 73-78
5. A. Akhtar, M.S. Hook, and R.C. Reed, On the Oxidation of the Third-Generation Single-Crystal Superalloy CMSX-10, *Metall. Mater. Trans. A*, 2005, **36A**, p 3001-3017
6. R. Orosz, U. Krupp, and H.J. Christ, Study of the Oxide Scale Integrity on Ni-Base Alloy CMSX-4 During Isothermal and Thermal-Cycling Exposure, *Mater. Corros.*, 2006, **57**, p 154-158
7. L. Höglund and J. Ågren, Analysis of the Kirkendall Effect, Marker Migration and Pore Formation, *Acta Mater.*, 2001, **49**, p 1311-1317
8. E. Perez, T. Patterson, and Y. Sohn, Interdiffusion Analysis for NiAl Versus Superalloys Diffusion Couples, *J. Phase Equilib. Diffus.*, 2006, **27**, p 659-664
9. A. Engström, J. Bratberg, Q. Chen, L. Höglund, P. Mason, Application of thermodynamic and kinetic modeling to diffusion simulations in nickel-base superalloy systems, in *Euro Superalloys 2010 (2011)*, p 198-203
10. N. Matan, H.M.A. Winand, P. Carter, M. Karunaratne, P.D. Bogdanoff, and R.C. Reed, A Coupled Thermodynamic/Kinetic Model for Diffusional Processes in Superalloys, *Acta Mater.*, 1998, **46**, p 4587-4600
11. M. Danielewski, R. Filipek, A. Milewska, Interdiffusion in oxidized multicomponent alloys, in *Diffusion and Reactions* ed. by M. Danielewski (2000), p 23-27
12. J.A. Nesbitt, COSIM—A finite-difference computer model to predict ternary concentration profiles associated with oxidation and interdiffusion of overlay-coated substrates, in *Lifetime Modelling of High Temperature Corrosion Processes (2001)*, p 359-378
13. W.M. Pragnell and H.E. Evans, A Finite-Difference Model to Predict 2D Depletion Profiles Arising from High Temperature Oxidation of Alloys, *Modell. Simul. Mater. Sci. Eng.*, 2006, **14**, p 733-740
14. H. Larsson and A. Engström, A Homogenization Approach to Diffusion Simulations Applied to Alpha + Gamma Fe-Cr-Ni Diffusion Couples, *Acta Mater.*, 2006, **54**, p 2431-2439
15. G.E. Fuchs, Solution Heat Treatment Response of a Third Generation Single Crystal Ni-base Superalloy, *Mater. Sci. Eng. A*, 2001, **300**, p 52-60
16. C. Schulze and M. Feller-Kniepmeier, Transmission Electron Microscopy of Phase Composition and Lattice Misfit in the Re-Containing Nickel-Base Superalloy CMSX-10, *Mater. Sci. Eng. A*, 2000, **281**, p 204-212
17. L. Onsager, Reciprocal Relations in Irreversible Processes. I, *Phys. Rev.*, 1931, **37**, p 405-426
18. T.J. Nijdam and W.G. Sloof, Modelling of Composition and Phase Changes in Multiphase Alloys Due to Growth of an Oxide Layer, *Acta Mater.*, 2008, **56**, p 4972-4983
19. A. Engström, L. Höglund, and J. Ågren, Computer-Simulation of Diffusion in Multiphase Systems, *Metall. Mater. Trans. A*, 1994, **25**, p 1127-1134
20. K. Bongartz, R. Schulten, W.J. Quadackers, and H. Nickel, A Finite-Difference Model Describing Carburization in High-Temperature Alloys, *Corrosion*, 1986, **42**, p 390-397
21. K. Bongartz, W.J. Quadackers, R. Schulten, and H. Nickel, A Mathematical-Model Describing Carburization in Multielement Alloy Systems, *Metall. Trans. A*, 1989, **20**, p 1021-1028

22. H.J. Christ, S.Y. Chang, and U. Krupp, Thermodynamic Characteristics and Numerical Modeling of Internal Nitridation of Nickel Base Alloys, *Mater. Corros.*, 2003, **54**, p 887-894
23. A. Borgenstam, A. Engström, L. Höglund, and J. Ågren, DICTRA, A Tool for Simulation of Diffusional Transformations in Alloys, *J. Phase Equilib.*, 2000, **21**, p 269-280
24. TCNi5, TCS Ni-based superalloys database v. 5.0 in 2012
25. MOBNi2, ThermoCalc Software Ni-alloys mobility database v. 2, in 2011
26. H. Nakajima, The Discovery and Acceptance of the Kirkendall Effect: The Result of a Short Research Career, *JOM*, 1997, **49**, p 15-19
27. C.E. Campbell, A New Technique for Evaluating Diffusion Mobility Parameters, *J. Equilib. Diff.*, 2005, **26**, p 435-440
28. A. Engström and J. Ågren, Assessment of Diffusional Mobilities in face-Centered Cubic Ni Cr Al Alloys, *Z. Metallkunde*, 1996, **87**, p 92-97
29. M.S.A. Karunaratne, P. Carter, and R.C. Reed, Interdiffusion in the Face-Centred Cubic Phase of the Ni-Re, Ni-Ta and Ni-W Systems Between 900 and 1300 °C, *Mater. Sci. Eng. A*, 2000, **281**, p 229-233
30. M. Hattori, N. Goto, Y. Murata, T. Koyama, and M. Morinaga, Diffusion of Refractory Elements in Ni-Al-X (X: Re, W) Ternary Alloys, *Mater. Trans.*, 2005, **46**, p 163-166
31. A.I. Epishin, A.O. Rodin, B.S. Bokshtein, G. Oder, T. Link, and I.L. Svetlov, Interdiffusion in Binary Ni-Re Alloys, *Phys. Met. Metall.*, 2015, **116**, p 1-7
32. M.S. Thompson and J.E. Morral, The Effect of Composition on Interdiffusion in Ternary Alloys, *Acta Metall.*, 1986, **34**, p 339-346
33. M.S. Thompson and J.E. Morral, The Square Root Diffusivity, *Acta Metall.*, 1986, **34**, p 2201-2203
34. M.S. Thompson and J.E. Morral, Using the Square Root Diffusivity to Predict Interdiffusion in the Ni-Cr-Al System, *J. Met.*, 1987, **39**, p A63
35. M.S. Thompson, J.E. Morral, and A.D. Romig, Applications of the Square Root Diffusivity to Diffusion in Ni-Al-Cr Alloys, *Metall. Trans. A*, 1990, **21**, p 2679-2685
36. C.E. Campbell, J.C. Zhao, and M.F. Henry, Comparison of Experimental and Simulated Multicomponent Ni-Base Superalloy Diffusion Couples, *J. Phase Equilib. Diff.*, 2004, **25**, p 6-15
37. N. Garimella, M.P. Brady, and Y. Sohn, Interdiffusion in Gamma (Face-Centered Cubic) Ni-Cr-X (X = Al, Si, Ge, or Pd) Alloys at 900 °C, *J. Phase Equilib. Diff.*, 2006, **27**, p 665-670
38. M. Hattori, N. Goto, Y. Murata, T. Koyama, and M. Morinaga, Diffusion of Refractory Elements in Ni-X-Y (X, Y: Re, W, Ru, Al) Ternary Alloys, *Mater. Trans.*, 2006, **47**, p 331-334
39. P.K. Gupta and A.R. Cooper, D matrix for Multicomponent Diffusion, *Physica*, 1971, **54**, p 39-59
40. TTNI7, TT Ni-based superalloys database in 2006
41. MOBNi1, TCS Ni-alloys mobility database, in 2006
42. A. Chyrkin, W.G. Sloof, R. Pillai, T. Galiullin, D. Grüner, and W.J. Quadackers, Modelling Compositional Changes in Nickel Base-Alloy 602 CA During High Temperature Oxidation, *Mater. High Temp.*, 2015, **32**, p 102-112
43. N.C. Oforka and B.B. Argent, Thermodynamics of Ni-Cr-Al Alloys, *J. Less-Common Met.*, 1985, **114**, p 97-109